The Aeronautical Journal (2026), 1–20
doi:10.1017/aer.2026.10233

ROYAL AERONAUTICAL SOCIETY

RESEARCH ARTICLE

Nonlinear model predictive control method for autonomous approach of tanker/receiver

He Song[2], Hao Fan[1], Ruohai Di[1], Xiaoyu Wang[2] and Shanshan Shi[2]

[1]Xi'an Technological University, China
[2]Xihang University, Xi'an, China
Corresponding author: Ruohai Di; Email: xfwtdrh@163.com

Received: 5 December 2025 UTC; **Revised:** 5 August 2026 UTC; **Accepted:** 5 August 2026 UTC

Keywords: autonomous aerial refueling; autonomous approaching; multivariable constraints; nonlinear model predictive control; adaptive gradient descent

Abstract

In order to solve the problems of strong nonlinearity, strong coupling and multivariable constraints of the receiverr's motion model in the process of the tanker/receiver autonomous approach, a nonlinear model predictive control (NMPC) method is proposed in this paper. By analysing the external forces and torques acting on the receiver, a nonlinear dynamic model of the receiver is established to provide an accurate prediction model for NMPC. An objective function with the terminal state of the receiver is designed, multiple state variable constraints are added, the adaptive gradient descent method is used to solve the optimal control quantity online and finally the stability of NMPC is proved. The numerical simulation results show that the proposed method has good control performance and can quickly and stably control the receiver to fly directly behind the tanker and maintain the same speed and direction.

Nomenclature

Symbol	Definition
AAR	Autonomous aerial refuelling
LQR, MPC, NMPC	Linear quadratic regulator, model predictive control and nonlinear model predictive control, respectively
UAV	Unmanned aerial vehicle
J	NMPC objective function
m	Mass of the receiver (kg)
N_p, N_u	Prediction- and control-horizon lengths, respectively
Q, R, S (NMPC)	State-error, control-input-increment and terminal-state-error weighting matrices, respectively
S (aerodynamics)	Reference wing area (m^2)
T	Sampling period (s)
$\vec{u}, \Delta\vec{u}$	Control-input vector and its increment, respectively
v_x, v_y, v_z	Body-axis velocity components (m/s)
V_a	Airspeed of the receiver (m/s)
x, y, z	Receiver position coordinates in the reference coordinate system (m)
$\vec{X}, \vec{X}_d, \hat{\vec{X}}$	Actual, reference and predicted state vectors, respectively
α, β	Angle of attack and sideslip angle, respectively (rad)
$\delta_a, \delta_e, \delta_r$	Aileron, elevator and rudder deflection angles, respectively (rad)
ρ	Air density (kg/m^3)
ϕ, θ, ψ	Roll, pitch and yaw Euler angles, respectively (rad)
$\omega_x, \omega_y, \omega_z$	Body-axis roll, pitch and yaw angular rates, respectively (rad/s)

© The Author(s), 2026. Published by Cambridge University Press on behalf of Royal Aeronautical Society.

https://doi.org/10.1017/aer.2026.10233 Published online by Cambridge University Press

1.0 Introduction

Autonomous aerial refueling (AAR) technology can expand the combat radius and extend the air holding time of unmanned aerial vehicles (UAVs), and is a multiplier of air power [1, 2]. In the process of AAR, it is necessary to study high-precision flight control methods to ensure that the receiver approaches the tanker autonomously and smoothly.

In recent years, the flight control problem of the receiver actively approaching the tanker has attracted the research interest of many scholars at home and abroad, and has achieved fruitful research results [3]. Burns and Lugo et al. generated the flight path using the Dubins curve method, and combined the nonlinear dynamic inverse control method and vector field theory to achieve the active approach of the receiver to the tanker [4–6]. Some scholars draw on the guidance idea of seeking to guide the receiver to fly autonomously to a safe position behind the tanker by designing guidance laws. For example, Ochi et al. improved the proportional guidance law and established a simple and feasible guidance method by controlling the line-of-sight angle [7]. Smith et al. improved the proportional guidance law based on adaptive terminal guidance, which not only solved the problem of autonomous approach of the receiver and tanker, but also analysed the influence of external disturbances [8]. Yoon and Kung et al. adopted the pure tracking guidance law and its improved method to achieve the autonomous approach of the receiver and tanker, improving the sensitivity and guidance during the approach [9, 10]. In addition to drawing on the idea of navigation guidance law, some scholars draw on the idea of guidance control rate to solve the problem of the receiverr's autonomous approach to the tanker. For example, Jun et al. improved the proportional guidance law based on the backstep control method to achieve terminal heading control and designed the control law of the altitude channel [11]. Dogan et al. designed a linear quadratic regulator (LQR) using the multi-input and multi-output state feedback method to achieve the autonomous approach of the receiver and tanker [12]. Schumacher et al. combined the adaptive control method, neural network method and dynamic inverse theory to design the control law of the flight motion of the receiver, achieving autonomous approach to the tanker [13]. Gong Quanquan and Yuan Suozhong et al. designed the guidance law and control law for the flight motion of the receiver based on the relationship between the position, speed and target line of sight between the tanker and receiver, achieving the autonomous approach of the two [14, 15].

Although the simulation results of the above-mentioned methods demonstrate the effectiveness of the designed guiding control method, it still can not well solve the problems of nonlinearity, strong coupling and multiple constrained variables existing in the dynamical model of the receiver. The model predictive control (MPC) method is a model-based finite-time-domain open-loop optimisation method. It uses the dynamic model of the controlled object to predict the future output of the system and combines rolling optimisation and feedback correction strategies. The performance indicators of the model are minimised within the constraint range to determine the optimal control quantity [16, 17]. However, during the rolling optimisation, the model needs to be linearised, and a precise nonlinear model of the system can not be accurately established, which is prone to cause the model mismatch problem [18, 19]. In view of the deficiencies of the MPC method, nonlinear model predictive control (NMPC) can make up for it well. It not only has good control performance for nonlinear models, but also can explicitly handle system constraints and solve non-convex programming problems [20]. Therefore, aiming at the characteristics of nonlinearity and multivariable constraints such as state and input variables in the motion model of the receiver during the receiver autonomous approach to the tanker, an autonomous approach method based on NMPC for tanker/receiver is proposed. The proposed method can quickly achieve the autonomous approach of the receiver and the tanker, and has good control performance.

The organisational structure of this paper is as follows. Section 2 conducts theoretical analysis and mathematical derivation of the in-air motion process of the receiver and establishes a nonlinear dynamic model of the receiver. Section 3 designs a NMPC method. The adaptive gradient descent method is adopted to solve the optimal control quantity online, and the convergence and closed-loop stability of the method are analysed by using the Lyapunov stability theory. Section 4 verified the validity and accuracy of the designed method through numerical simulation; Section 5 summarises and generalises the research work done.

https://doi.org/10.1017/aer.2026.10233 Published online by Cambridge University Press

2.0 Nonlinear dynamic model of the unmanned receiver

Based on the background of AAR of UAVs, this paper mainly studies the control methods for the receiver to autonomously approach the tanker. Therefore, establishing an accurate dynamic model of the receiver is the primary task. The receiver system is complex, nonlinear and strongly coupled. Its motion can be divided into two parts: the motion of the centre of mass and the rotation around the centre of mass, namely three linear motions and three angular motions [3, 21]. In this section, a set of multi-dimensional state variables $\vec{X} = [x, y, z, v_x, v_y, v_z, \varphi, \theta, \psi, \omega_x, \omega_y, \omega_z]^T$ will be selected. This set of state variables contains the position information of the receiver in the geocentric coordinate system, as well as the velocity, attitude angle and angular velocity information in the body coordinate system, in order to establish the dynamic model of the receiver. Before establishing the dynamic model of the receiver, it is necessary to analyse and model the forces and moments acting on it during its motion process.

2.1 Analysis of force and torque

During the flight of the receiver in the air, The receiver is subjected to different external forces. The common external forces mainly include the gravitational force $\vec{G}$, the thrust $\vec{f}$ of the receiver and the total aerodynamic force $\vec{A}$. It is precisely because of the combined effect of these external forces that the receiver can achieve different manoeuvres in the air. The different external forces acting on the receiver have different effects and properties. Next, we will analyse and model these different external forces.

2.1.1 Gravity

The receiver is always affected by the force of gravity during flight, and the direction is always vertically downward. During the AAR process, the flight altitude of the receiver is usually between 4 and 10 km [21]. The influence of altitude on the gravitational force acting on the receiver can be ignored and assumed as a constant vector. In the geocentric coordinate system, the gravitational force $\vec{G}$ can be expressed as [22]:

$$\vec{G} = m\begin{bmatrix} 0 & 0 & g \end{bmatrix}^T \tag{1}$$

where g is the gravitational acceleration, and $g = 9.8\, m/s^2$ is a constant.

According to the transformation relationship between the geocentric coordinate system and the body coordinate system of the receiver [22], the expression of gravity in the body coordinate system can be obtained:

$$\begin{aligned} \vec{F}_G^b = C_g^b \vec{G} &= m \begin{bmatrix} \cos\theta\cos\psi & \cos\theta\sin\psi & -\sin\theta \\ \sin\theta\cos\psi\sin\varphi - \sin\psi\cos\varphi & \sin\theta\sin\psi\sin\varphi + \cos\psi\cos\varphi & \cos\theta\sin\varphi \\ \sin\theta\cos\psi\cos\varphi + \sin\psi\sin\varphi & \sin\theta\sin\psi\cos\varphi - \cos\psi\sin\varphi & \cos\theta\cos\varphi \end{bmatrix} \begin{bmatrix} 0 \\ 0 \\ g \end{bmatrix} \\ &= m \begin{bmatrix} -g\sin\theta \\ g\cos\theta\sin\varphi \\ g\cos\theta\cos\varphi \end{bmatrix} \end{aligned} \tag{2}$$

where C_g^b is the rotation matrix from the geocentric coordinate system to the body coordinate system of the receiver; (φ, θ, ψ) are the roll angle, pitch angle and yaw angle of the receiver, respectively.

The gravitational force acting on the receiver is evenly distributed throughout the body of the receiver. The resultant gravitational force acts on the centre of the body of the receiver and does not generate a gravitational moment. Therefore, the moment of gravity in the body coordinate system of the receiver can be expressed as:

$$\vec{M}_G^b = \begin{bmatrix} 0 & 0 & 0 \end{bmatrix}^T \tag{3}$$

https://doi.org/10.1017/aer.2026.10233 Published online by Cambridge University Press

2.1.2 Thrust

The thrust received by the receiver is used to overcome the air resistance and control the flight speed and altitude. Imagine the engine of the receiver is a vector engine. In the body coordinate system of the receiver, the thrust can be expressed as:

$$\vec{F}_f^b = \left[f_x,\ f_y,\ f_z\right]^T \tag{4}$$

When the engine is installed at a certain position away from the centre of the receiver, it will cause the thrust to generate a corresponding thrust torque relative to the origin of the body coordinate system of the receiver. In the body coordinate system of the receiver, suppose the distances from each component of the thrust to the centre of mass of the receiver are l_x, l_y and l_z, respectively. According to the relationship between torque and force, the expression of the torque generated by the thrust is:

$$\vec{M}_f^b = \left[l_x f_x, l_y f_y, l_z f_z\right]^T \tag{5}$$

2.1.3 Aerodynamics

The receiver will generate aerodynamics under the action of airflow during flight. In the airflow coordinate system, the components of the aerodynamic forces acting on the receiver along the $o_v x_v$ axis, $o_v y_v$ axis and $o_v z_v$ axis are usually represented by drag D, lateral force Y and lift L. The aerodynamic force received by the receiver can be divided into longitudinal aerodynamic force and transverse aerodynamic force.

2.1.3.1 Longitudinal aerodynamics. Longitudinal aerodynamics mainly affect the movement of the receiver in the $o_b x_b z_b$ plane of the body coordinate system, and the involved aerodynamics are drag D and lift L. The main variables affecting longitudinal aerodynamics are the attack angle α, the pitch angle velocity ω_y and the elevator deflection angle δ_e of the receiver. In the airflow coordinate system, the expression of the longitudinal aerodynamic force acting on the receiver is [16]:

$$\begin{cases} D = \dfrac{1}{2}\rho V_a^2 S\left(C_D(\alpha) + C_{D_{\omega_y}}\dfrac{c}{2V_a}\omega_y + C_{D_{\delta_e}}\delta_e\right) \\ L = \dfrac{1}{2}\rho V_a^2 S\left(C_L(\alpha) + C_{L_{\omega_y}}\dfrac{c}{2V_a}\omega_y + C_{L_{\delta_e}}\delta_e\right) \end{cases} \tag{6}$$

where ρ is the density of air, calculated by the formula $\rho = 1.293^*$ (actual pressure/standard physical atmospheric pressure)* (273.15/actual absolute temperature), and under standard conditions, ρ is usually taken as 1.293 kg/m^3; V_a is the airspeed of the receiver; S is the reference area of the receiver wing; c is the average aerodynamic chord length of the receiver wing. For the calculation, formulas of $C_D(\alpha)$ and $C_L(\alpha)$, can be seen the reference [16].

According to the transformation relationship between the airflow coordinate system and the body coordinate system of the receiver [22], the expressions of drag D and lift L in the body coordinate system can be obtained:

$$\begin{bmatrix} F_{A_x}^b \\ F_{A_z}^b \end{bmatrix} = \begin{bmatrix} \cos\alpha & -\sin\alpha \\ \sin\alpha & \cos\alpha \end{bmatrix}\begin{bmatrix} -D \\ -L \end{bmatrix} = \frac{1}{2}\rho V_a^2 S\begin{bmatrix} C_X(\alpha) + C_{X_{\omega_y}}(\alpha)\dfrac{c}{2V_a}\omega_y + C_{X_{\delta_e}}(\alpha)\delta_e \\ C_Z(\alpha) + C_{Z_{\omega_y}}(\alpha)\dfrac{c}{2V_a}\omega_y + C_{Z_{\delta_e}}(\alpha)\delta_e \end{bmatrix} \tag{7}$$

where $C_X(\alpha) = -C_D(\alpha)\cos\alpha + C_L(\alpha)\sin\alpha$; $C_{X_{\omega_y}}(\alpha) = -C_{D_{\omega_y}}\cos\alpha + C_{L_{\omega_y}}\sin\alpha$; $C_{X_{\delta_e}}(\alpha) = -C_{D_{\delta_e}}\cos\alpha + C_{L_{\delta_e}}\sin\alpha$; $C_Z(\alpha) = -C_D(\alpha)\sin\alpha - C_L(\alpha)\cos\alpha$; $C_{Z_{\omega_y}}(\alpha) = -C_{D_{\omega_y}}\sin\alpha + C_{L_{\omega_y}}\cos\alpha$; $C_{Z_{\delta_e}}(\alpha) = -C_{D_{\delta_e}}\sin\alpha - C_{L_{\delta_e}}\cos\alpha$.

2.1.3.2 Lateral aerodynamics. The lateral aerodynamic force mainly affects the movement of the receiver in the $o_b y_b$ axis direction of the body coordinate system, and simultaneously influences the rolling and yaw movements of the receiver. The involved aerodynamic force is the lateral force Y. The main variables affecting lateral aerodynamics are the side-slip angle β, the rolling angular velocity ω_x,

https://doi.org/10.1017/aer.2026.10233 Published online by Cambridge University Press

the yaw angular velocity ω_z, the aileron rudder deflection angle δ_a and the rudder deflection angle δ_r of the receiver. In the body coordinate system, the expression of the lateral aerodynamic force acting on the receiver is [16]:

$$F_{A_y}^b = \frac{1}{2}\rho V_a^2 S\left(C_{Y_0} + C_{Y_\beta}\beta + C_{Y_{\omega_x}}\frac{b}{2V_a}\omega_x + C_{Y_{\omega_z}}\frac{b}{2V_a}\omega_z + C_{Y_{\delta_a}}\delta_a + C_{Y_{\delta_r}}\delta_r\right) \tag{8}$$

where b is the wingspan of the receiver wing; $C_{Y_0}, C_{Y_\beta}, C_{Y_{\omega_x}}, C_{Y_{\omega_z}}, C_{Y_{\delta_a}}$ and $C_{Y_{\delta_r}}$ are all coefficients.

Therefore, in the body coordinate system, the expression of the total aerodynamic force acting on the receiver is:

$$\vec{F}_A^b = \begin{bmatrix} F_{A_x}^b \\ F_{A_y}^b \\ F_{A_z}^b \end{bmatrix} = \frac{1}{2}\rho V_a^2 S\begin{bmatrix} C_X(\alpha) + C_{X_{\omega_y}}(\alpha)\dfrac{c}{2V_a}\omega_y + C_{X_{\delta_e}}(\alpha)\delta_e \\ C_{Y_0} + C_{Y_\beta}\beta + C_{Y_{\omega_x}}\dfrac{b}{2V_a}\omega_x + C_{Y_{\omega_z}}\dfrac{b}{2V_a}\omega_z + C_{Y_{\delta_a}}\delta_a + C_{Y_{\delta_r}}\delta_r \\ C_Z(\alpha) + C_{Z_{\omega_y}}(\alpha)\dfrac{c}{2V_a}\omega_y + C_{Z_{\delta_e}}(\alpha)\delta_e \end{bmatrix} \tag{9}$$

Correspondingly, the expression of the aerodynamic torque acting on the receiver in the body coordinate system can be obtained [22]:

$$\vec{M}_A^b = \begin{bmatrix} M_{A_x}^b \\ M_{A_y}^b \\ M_{A_z}^b \end{bmatrix} = \frac{1}{2}\rho V_a^2 S\begin{bmatrix} b\left(C_{x_0} + C_{x_\beta}\beta + C_{x_{\omega_x}}\dfrac{b}{2V_a}\omega_x + C_{x_{\omega_z}}\dfrac{b}{2V_a}\omega_z + C_{x_{\delta_a}}\delta_a + C_{x_{\delta_r}}\delta_r\right) \\ c\left(C_{y_0} + C_{y_\alpha}\alpha + C_{y_{\omega_y}}\dfrac{b}{2V_a}\omega_y + C_{y_{\delta_e}}\delta_e\right) \\ b\left(C_{z_0} + C_{z_\beta}\beta + C_{z_{\omega_x}}\dfrac{b}{2V_a}\omega_x + C_{z_{\omega_z}}\dfrac{b}{2V_a}\omega_z + C_{z_{\delta_a}}\delta_a + C_{z_{\delta_r}}\delta_r\right) \end{bmatrix} \tag{10}$$

Based on the above analysis, it can be known that in the body coordinate system, the expressions of the resultant external force $\vec{F}^b$ and the resultant external torque $\vec{M}^b$ acting on the receiver are:

$$\begin{aligned} \vec{F}^b &= \vec{F}_G^b + \vec{F}_f^b + \vec{F}_A^b = mg\begin{bmatrix} -\sin\theta \\ \cos\theta\sin\varphi \\ \cos\theta\cos\varphi \end{bmatrix} \\ &+ \begin{bmatrix} f_x \\ f_y \\ f_z \end{bmatrix} + \frac{1}{2}\rho V_a^2 S\begin{bmatrix} C_X(\alpha) + C_{X_{\omega_y}}(\alpha)\dfrac{c}{2V_a}\omega_y + C_{X_{\delta_e}}(\alpha)\delta_e \\ C_{Y_0} + C_{Y_\beta}\beta + C_{Y_{\omega_x}}\dfrac{b}{2V_a}\omega_x + C_{Y_{\omega_z}}\dfrac{b}{2V_a}\omega_z + C_{Y_{\delta_a}}\delta_a + C_{Y_{\delta_r}}\delta_r \\ C_Z(\alpha) + C_{Z_{\omega_y}}(\alpha)\dfrac{c}{2V_a}\omega_y + C_{Z_{\delta_e}}(\alpha)\delta_e \end{bmatrix} \end{aligned} \tag{11}$$

$$\begin{aligned} \vec{M}^b &= \vec{M}_G^b + \vec{M}_f^b + \vec{M}_A^b \\ &= \begin{bmatrix} l_x f_x \\ l_y f_y \\ l_x f_z \end{bmatrix} + \frac{1}{2}\rho V_a^2 S\begin{bmatrix} b\left(C_{x_0} + C_{x_\beta}\beta + C_{x_{\omega_x}}\dfrac{b}{2V_a}\omega_x + C_{x_{\omega_z}}\dfrac{b}{2V_a}\omega_z + C_{x_{\delta_a}}\delta_a + C_{x_{\delta_r}}\delta_r\right) \\ c\left(C_{y_0} + C_{y_\alpha}\alpha + C_{y_{\omega_y}}\dfrac{b}{2V_a}\omega_y + C_{y_{\delta_e}}\delta_e\right) \\ b\left(C_{z_0} + C_{z_\beta}\beta + C_{z_{\omega_x}}\dfrac{b}{2V_a}\omega_x + C_{z_{\omega_z}}\dfrac{b}{2V_a}\omega_z + C_{z_{\delta_a}}\delta_a + C_{z_{\delta_r}}\delta_r\right) \end{bmatrix} \end{aligned} \tag{12}$$

2.2 Dynamic model of the receiver

Through the analysis of the forces and torques acting on the receiver in Section 2.1, this section will respectively establish the translational dynamics model of the centre of mass and the rotational dynamics

https://doi.org/10.1017/aer.2026.10233 Published online by Cambridge University Press

model around the centre of mass of the receiver in the body coordinate system based on Newtonr's laws of motion and the theorem of moments of motion.

2.2.1 Translational dynamics model of the centre of mass

The receiver's body coordinate system is adopted as the moving reference frame, and its velocity vector relative to the geocentric coordinate system is $\vec{V}$, and the angular velocity vector of rotation is $\vec{\omega}$. According to the relationship between the absolute derivative and the relative derivative of a vector expression, in a dynamic coordinate system, the expression for differentiating the velocity vector $\vec{V}$ with respect to time is [3]:

$$\frac{d\vec{V}}{dt} = \frac{\delta\vec{V}}{\delta t} + \vec{\omega} \times \vec{V} \tag{13}$$

where $\frac{d\vec{V}}{dt}$ represents the absolute derivative of the velocity vector $\vec{V}$ in the geocentric coordinate system; $\frac{\delta\vec{V}}{\delta t}$ represents the relative derivative of the velocity vector $\vec{V}$ in the machine coordinate system.

In the body coordinate system, $\vec{V} = [v_x, v_y, v_z]^T$ is the velocity vector and $\vec{\omega} = [\omega_x, \omega_y, \omega_z]^T$ is the angular velocity vector. Substituting them into Equation (13), we can obtain:

$$\frac{d\vec{V}}{dt} = \begin{bmatrix} \dot{v}_x \\ \dot{v}_y \\ \dot{v}_z \end{bmatrix} + \begin{bmatrix} \omega_x \\ \omega_y \\ \omega_z \end{bmatrix} \times \begin{bmatrix} v_x \\ v_y \\ v_z \end{bmatrix} = \begin{bmatrix} \dot{v}_x + \omega_y v_z - \omega_z v_y \\ \dot{v}_y + \omega_z v_x - \omega_x v_z \\ \dot{v}_z + \omega_x v_y - \omega_y v_x \end{bmatrix} \tag{14}$$

In the body coordinate system, $\vec{F}^b = [F_x^b, F_y^b, F_z^b]^T$ is the resultant external force acting on the receiver, according to Newtonr's laws of motion, after calculation and organisation, Equation (14) can be rewritten as:

$$\begin{cases} \dot{v}_x = \dfrac{F_x^b}{m} + \omega_z v_y - \omega_y v_z \\ \dot{v}_y = \dfrac{F_y^b}{m} - \omega_z v_x + \omega_x v_z \\ \dot{v}_z = \dfrac{F_z^b}{m} + \omega_y v_x - \omega_x v_y \end{cases} \tag{15}$$

where m represents the mass of the receiver.

Combining Equation (11), the translational dynamics model of the centre of mass of the receiver in the body coordinate system can be obtained:

$$\begin{bmatrix} \dot{v}_x \\ \dot{v}_y \\ \dot{v}_z \end{bmatrix} = \begin{bmatrix} \omega_z v_y - \omega_y v_z \\ \omega_x v_z - \omega_z v_x \\ \omega_y v_x - \omega_x v_y \end{bmatrix}$$

$$+ \begin{bmatrix} -g\sin\theta + \dfrac{f_x}{m} + \dfrac{1}{2m}\rho V_a^2 S\left(C_X(\alpha) + C_{X_{\omega_y}}(\alpha)\dfrac{c}{2V_a}\omega_y + C_{X_{\delta_e}}(\alpha)\delta_e\right) \\ g\cos\theta\sin\varphi + \dfrac{f_y}{m} + \dfrac{1}{2m}\rho V_a^2 S\left(C_{Y_0} + C_{Y_\beta}\beta + C_{Y_{\omega_x}}\dfrac{b}{2V_a}\omega_x + C_{Y_{\omega_z}}\dfrac{b}{2V_a}\omega_z + C_{Y_{\delta_a}}\delta_a + C_{Y_{\delta_r}}\delta_r\right) \\ g\cos\theta\cos\varphi + \dfrac{f_z}{m} + \dfrac{1}{2m}\rho V_a^2 S\left(C_Z(\alpha) + C_{Z_{\omega_y}}(\alpha)\dfrac{c}{2V_a}\omega_y + C_{Z_{\delta_e}}(\alpha)\delta_e\right) \end{bmatrix} \tag{16}$$

2.2.2 Rotational dynamics model around the centre of mass

Similarly, taking the body coordinate system of the receiver as the dynamic coordinate system, based on the relationship between the absolute derivative and the relative derivative of the vector expression,

https://doi.org/10.1017/aer.2026.10233 Published online by Cambridge University Press

the derivative of the angular momentum $\vec{H}$ with respect to time can be expressed as [3]:

$$\frac{d\vec{H}}{dt} = \frac{\delta\vec{H}}{\delta t} + \vec{\omega} \times \vec{H} \tag{17}$$

where $\frac{d\vec{H}}{dt}$ represents the absolute derivative of angular momentum $\vec{H}$ in the geocentric coordinate system; $\frac{\delta\vec{H}}{\delta t}$ represents the relative derivative of the angular momentum $\vec{H}$ in the body coordinate system.

In the body coordinate system, the angular momentum $\vec{H}$ can be expressed as [3]:

$$\vec{H} = \vec{J} \cdot \vec{\omega} = \begin{bmatrix} J_x & -J_{xy} & -J_{xz} \\ -J_{xy} & J_y & -J_{yz} \\ -J_{xz} & -J_{yz} & J_z \end{bmatrix} \begin{bmatrix} \omega_x \\ \omega_y \\ \omega_z \end{bmatrix} = \begin{bmatrix} J_x\omega_x - J_{xy}\omega_y - J_{xz}\omega_z \\ -J_{xy}\omega_x + J_y\omega_y - J_{yz}\omega_z \\ -J_{xz}\omega_x - J_{yz}\omega_y + J_z\omega_z \end{bmatrix} \tag{18}$$

where J_x, J_y and J_z, respectively, represent the moments of inertia of the receiver around the three axes o_bx_b, o_by_b and o_bz_b of the body coordinate system, as well as the products of inertia J_{xy}, J_{yx}, J_{xz}, J_{zx}, J_{yz} and J_{zy}. And its calculation formulas are as follows [3].

$$\begin{cases} J_x = \int (y^2 + z^2)dm; J_y = \int (x^2 + z^2)dm; J_z = \int (y^2 + x^2)dm \\ J_{xy} = \int (xy)dm = J_{yx}; J_{xz} = \int (xz)dm = J_{zx}; J_{yz} = \int (yz)dm = J_{zy} \end{cases} \tag{19}$$

The receiver belongs to the face weight type of UAV, and its inertial products J_{xy}=J_{yx}=J_{yz}=J_{zy} = 0. Equation (19) can be rewritten as:

$$\vec{H} = \vec{J} \cdot \vec{\omega} = \begin{bmatrix} J_x & 0 & -J_{xz} \\ 0 & J_y & 0 \\ -J_{xz} & 0 & J_z \end{bmatrix} \begin{bmatrix} \omega_x \\ \omega_y \\ \omega_z \end{bmatrix} = \begin{bmatrix} J_x\omega_x - J_{xz}\omega_z \\ J_y\omega_y \\ -J_{xz}\omega_x + J_z\omega_z \end{bmatrix} \tag{20}$$

In the body coordinate system, $\vec{M}^b = [M_x^b, M_y^b, M_z^b]^T$ represents the resultant external torque acting on the receiver. According to the theorem of moment of motion, combined with Equations (17) and (20), after calculation and organisation, it can be obtained as follows:

$$\begin{bmatrix} \dot{\omega}_x \\ \dot{\omega}_y \\ \dot{\omega}_z \end{bmatrix} = \begin{bmatrix} J_x & 0 & -J_{xz} \\ 0 & J_y & 0 \\ -J_{xz} & 0 & J_z \end{bmatrix}^{-1} \left(\begin{bmatrix} M_x^b \\ M_y^b \\ M_z^b \end{bmatrix} - \begin{bmatrix} (J_z - J_y)\omega_y\omega_z - J_{xz}\omega_x\omega_y \\ (J_x - J_z)\omega_x\omega_z + J_{xz}\left(\omega_x^2 - \omega_y^2\right) \\ (J_y - J_x)\omega_x\omega_y + J_{xz}\omega_y\omega_z \end{bmatrix} \right) \tag{21}$$

Combining Equation (12), the rotational dynamics model of the receiver around the centre of mass in the body coordinate system can be obtained:

$$\begin{bmatrix} \dot{\omega}_x \\ \dot{\omega}_y \\ \dot{\omega}_z \end{bmatrix} = \vec{\Gamma} \cdot \begin{bmatrix} J_{xz}\omega_x\omega_y - (J_z - J_y)\omega_y\omega_z \\ J_{xz}\left(\omega_y^2 - \omega_x^2\right) - (J_x - J_x)\omega_x\omega_z \\ -J_{xz}\omega_y\omega_z - (J_y - J_x)\omega_x\omega_y \end{bmatrix} + \vec{\Gamma} \cdot \begin{bmatrix} l_x f_x \\ l_y f_y \\ l_x f_z \end{bmatrix}$$

$$+ \vec{\Gamma} \cdot \frac{1}{2}\rho V_a^2 S \begin{bmatrix} b\left(C_{x_0} + C_{x_\beta}\beta + C_{x_{\omega x}}\frac{b}{2V_a}\omega_x + C_{x_{\omega z}}\frac{b}{2V_a}\omega_z + C_{x_{\delta a}}\delta_a + C_{x_{\delta r}}\delta_r \right) \\ c\left(C_{y_0} + C_{y_\alpha}\alpha + C_{y_{\omega y}}\frac{b}{2V_a}\omega_y + C_{y_{\delta e}}\delta_e \right) \\ b\left(C_{z_0} + C_{z_\beta}\beta + C_{z_{\omega x}}\frac{b}{2V_a}\omega_x + C_{z_{\omega z}}\frac{b}{2V_a}\omega_z + C_{z_{\delta a}}\delta_a + C_{z_{\delta r}}\delta_r \right) \end{bmatrix} \tag{22}$$

https://doi.org/10.1017/aer.2026.10233 Published online by Cambridge University Press

$$\text{where } \vec{\Gamma} = \begin{bmatrix} J_x & 0 & -J_{xz} \\ 0 & J_y & 0 \\ -J_{xz} & 0 & J_z \end{bmatrix}^{-1} = \frac{1}{J_x J_y J_z - J_y J_{xz}^2} \begin{bmatrix} J_y J_z & 0 & J_y J_{xz} \\ 0 & J_x J_z - J_{xz}^2 & 0 \\ J_y J_{xz} & 0 & J_x J_y \end{bmatrix}.$$

To establish the dynamic model of the receiver with complete state variables, it is also necessary to respectively provide the positional motion model of the receiver in the geocentric coordinate system and the angular rotation model in the body coordinate system [21]:

$$\begin{bmatrix} \dot{x} \\ \dot{y} \\ \dot{z} \end{bmatrix} = \begin{bmatrix} \cos\theta\cos\psi v_x + (\sin\theta\cos\psi\sin\varphi - \sin\psi\cos\varphi)\, v_y + (\sin\theta\cos\psi\cos\varphi + \sin\psi\sin\varphi)\, v_z \\ \cos\theta\sin\psi v_x + (\sin\theta\sin\psi\sin\varphi - \cos\psi\cos\varphi)\, v_y + (\sin\theta\sin\psi\cos\varphi - \cos\psi\sin\varphi)\, v_z \\ \sin\theta v_x - \cos\theta\sin\varphi v_y - \cos\theta\cos\varphi v_z \end{bmatrix} \tag{23}$$

$$\begin{cases} \dot{\varphi} = \omega_x + \tan\theta(\omega_y\sin\varphi + \omega_z\cos\varphi) \\ \dot{\theta} = \omega_y\cos\varphi - \omega_z\sin\varphi \\ \dot{\psi} = \sec\theta(\omega_y\sin\varphi + \omega_z\cos\varphi) \end{cases} \tag{24}$$

Combining Equations (16) and (22) to (24), when $\vec{X} = [x, y, z, v_x, v_y, v_z, \varphi, \theta, \psi, \omega_x, \omega_y, \omega_z]^T$ is taken as the state variable, $\vec{u} = [f_x, f_y, f_z, \delta_a, \delta_e, \delta_r]^T$ is taken as the control variable, the dynamic model of the receiver can be expressed as:

$$\dot{\vec{X}}(t) = f(\vec{X}(t), \vec{u}(t)) \tag{25}$$

where $f(\vec{X}(t), \vec{u}(t)) = [A_{3\times1}, B_{3\times1}, C_{3\times1}, D_{3\times1}]^T$;

$$A_{3\times1} = \begin{bmatrix} \cos\theta\cos\psi v_x + (\sin\theta\cos\psi\sin\varphi - \sin\psi\cos\varphi)v_y + (\sin\theta\cos\psi\cos\varphi + \sin\psi\sin\varphi)v_z \\ \cos\theta\sin\psi v_x + (\sin\theta\sin\psi\sin\varphi - \cos\psi\cos\varphi)v_y + (\sin\theta\sin\psi\cos\varphi - \cos\psi\sin\varphi)v_z \\ \sin\theta v_x - \cos\theta\sin\varphi v_y - \cos\theta\cos\varphi v_z \end{bmatrix};$$

$$B_{3\times1} = \begin{bmatrix} \omega_z v_y - \omega_y v_z - g\sin\theta + \frac{f_x}{m} + \frac{d}{m}\left(C_X(\alpha) + C_{X_{\omega_y}}(\alpha)\frac{c}{2V_a}\omega_y + C_{X_{\delta_e}}(\alpha)\delta_e\right) \\ \omega_x v_z - \omega_z v_x + g\cos\theta\sin\varphi + \frac{f_x}{m} + \frac{d}{m}\left(C_{Y_0} + C_{Y_\beta}\beta + C_{Y_{\omega_x}}\frac{b}{2V_a}\omega_x + C_{Y_{\omega_z}}\frac{b}{2V_a}\omega_z + C_{Y_{\delta_a}}\delta_a + + C_{Y_{\delta_r}}\delta_r\right) \\ \omega_y v_x - \omega_x v_y - g\cos\theta\cos\varphi + \frac{f_z}{m} + \frac{d}{m}\left(C_Z(\alpha) + C_{Z_{\omega_y}}(\alpha)\frac{c}{2V_a}\omega_y + C_{Z_{\delta_e}}(\alpha)\delta_e\right) \end{bmatrix};$$

$$C_{3\times1} = \begin{bmatrix} \omega_x + \tan\theta(\omega_y\sin\varphi + \omega_z\cos\varphi) \\ \omega_y\cos\varphi - \omega_z\sin\varphi \\ \sec\theta(\omega_y\sin\varphi + \omega_z\cos\varphi) \end{bmatrix};$$

$$D_{3\times1} = \begin{bmatrix} \frac{\left(J_y J_z J_{xz} - J_y^2 J_{xz} + J_x J_y J_{xz}\right)\omega_x\omega_y - \left(J_y J_z^2 - J_y^2 J_z + J_y J_{xz}^2\right)\omega_y\omega_z}{J_x J_y J_z - J_y J_{xz}^2} \\ \frac{\left(J_x J_z J_{xz} - J_{xz}^3\right)\left(\omega_y^2 - \omega_x^2\right) - \left(J_x J_z - J_{xz}^2\right)(J_x - J_x)\,\omega_x\omega_z}{J_x J_y J_z - J_y J_{xz}^2} \\ \frac{\left(J_y J_{xz}^2 - J_x J_y^2 + J_x^2 J_y\right)\omega_x\omega_y - \left(J_y J_z J_{xz} - J_y^2 J_{xz} + J_x J_y J_{xz}\right)\omega_y\omega_z}{J_x J_y J_z - J_y J_{xz}^2} \end{bmatrix}$$

$$+ \vec{\Gamma}\begin{bmatrix} l_x f_x + db\left(C_{x_0} + C_{x_\beta}\beta + C_{x_{\omega x}}\frac{b}{2V_a}\omega_x + C_{x_{\omega z}}\frac{b}{2V_a}\omega_z + C_{x_{\delta a}}\delta_a + C_{x_{\delta r}}\delta_r\right) \\ l_y f_y + dc\left(C_{y_0} + C_{x_\alpha}\alpha + C_{y_{\omega_y}}\frac{b}{2V_a}\omega_y + C_{y_{\delta_e}}\delta_e\right) \\ l_z f_z + db\left(C_{z_0} + C_{z_\beta}\beta + C_{z_{\omega x}}\frac{b}{2V_a}\omega_x + C_{z_{\omega z}}\frac{b}{2V_a}\omega_z + C_{z_{\delta_a}}\delta_a + C_{z_{\delta r}}\delta_r\right) \end{bmatrix}.$$

https://doi.org/10.1017/aer.2026.10233 Published online by Cambridge University Press

In addition, during the process of refueling operations, the receiver will be affected by atmospheric turbulence. The Dryden model is a commonly used atmospheric turbulence model in flight control, and its descriptive equation is [21]:

$$\begin{cases} \Phi_x = \sigma_x^2 \cdot \dfrac{L_x}{\pi} \cdot \dfrac{1}{1+(L_x\Omega)^2} \\ \Phi_y = \sigma_y^2 \cdot \dfrac{L_y}{\pi} \cdot \dfrac{1+12(L_y\Omega)^2}{[1+4(L_y\Omega)^2]^2} \\ \Phi_z = \sigma_z^2 \cdot \dfrac{L_z}{\pi} \cdot \dfrac{1+12(L_z\Omega)^2}{[1+4(L_z\Omega)^2]^2} \end{cases} \tag{26}$$

where Φ_x, Φ_y and Φ_z are the three-axis spectral functions of atmospheric turbulence in the body coordinate system; Ω is the spatial frequency of atmospheric turbulence; σ_x, σ_y and σ_z are the turbulence intensity at a certain height and $\sigma_x = \sigma_y = \sigma_z$; L_x, L_y and L_z are the turbulence scale at a certain height, and L_x=L_y=L_z.

The atmospheric turbulence can be seen as external uncertainty disturbances experienced by the receiver. Therefore, Equation (25) can be rewritten as

$$\dot{\vec{X}}(t) = f(\vec{X}(t), \vec{u}(t)) + \varepsilon(t) \tag{27}$$

where $\varepsilon(t)$ represents external uncertainty disturbances that include atmospheric turbulence.

At this point, through the analysis of the motion process of the receiver, the nonlinear dynamic model of the receiver as shown in Equation (27) is obtained. Our target is to design a controller based on the nonlinear model of Equation (27) to enable the receiver to actively approach the tanker smoothly and rapidly. It is required that the final flight speed and attitude of the receiver when successfully approaching the tanker be the same as those of the tanker, and maintain a certain safety distance and height deviation from the tanker.

3.0 Design of the NMPC method

In the actual process of AAR, we expect the receiver to approach the tanker actively and quickly in a short time and with low fuel consumption. This can not only save the aerial refueling time and improve the success rate of the receiver in performing subsequent tasks, but also reduce the exposure time of the tanker/receiver in the air, ensuring the safety of the two UAVs. Essentially, the approach control problem of the tanker/receiver can be regarded as an optimal control problem, that is, to seek an optimal control quantity $\vec{u}^*(t)$ so that the approach control time of the tanker/receiver is short and the fuel consumption is low. This section will adopt the NMPC method to solve the optimal control problem of the active approach of the receiver to the tanker.

3.1 Objective function

NMPC is usually described in two forms: the discrete-time model and the continuous-time model. Compared with the continuous-time model, the discrete-time model is more robust in the case of small sample time intervals [23]. Therefore, the prediction model in the discrete-time state is used. Assuming the sampling time is T, the dynamic model of the receiver in the discrete-time state in the form of Equation (28) is shown as follows.

$$\begin{cases} \vec{X}(k+1) = \vec{X}(k) + T \cdot f(\vec{X}(k), \Delta\vec{u}(k)) + \vec{\varepsilon}(k) \\ \vec{u}(k) = \vec{u}(k-1) + \Delta\vec{u}(k) \end{cases} \tag{28}$$

where k is the sampling moment; $\Delta\vec{u}(k)$ is the increment of the control input.

https://doi.org/10.1017/aer.2026.10233 Published online by Cambridge University Press

Assuming that $\vec{\varepsilon}(k)$ remains constant in the predicted time domain, the following form of objective function can be established:

$$\begin{aligned} J = & \sum_{i=1}^{N_p-1} \left[\vec{X}_d(k+i|k) - \hat{\vec{X}}(k+i|k)\right]^T Q\left[\vec{X}_d(k+i|k) - \hat{\vec{X}}(k+i|k)\right] \\ & + \sum_{i=0}^{N_u-1} (\Delta\vec{u})^T (k+i|k) R (\Delta\vec{u}) (k+i|k) \\ & + \left[\vec{X}_d(k+N_p|k) - \hat{\vec{X}}(k+N_p|k)\right]^T S\left[\vec{X}_d(k+N_p|k) - \hat{\vec{X}}(k+N_p|k)\right] \end{aligned} \tag{29}$$

where the first item and the second item are respectively the state cost and control input cost functions, which realise the active approach control from the receiver to the tanker; the third item is the terminal state cost function, which is used to ensure the stability of the NMPC controller; $[\vec{X}_d(k+1|k), \vec{X}_d(k+2|k), \cdots, \vec{X}_d(k+N_p|k)]^T$ is the reference value of the state vector of the receiver at time k, which can be obtained from the output value of the dynamic model of the tanker; $[\hat{\vec{X}}(k+1|k), \hat{\vec{X}}(k+2|k), \cdots, \hat{\vec{X}}(k+N_p|k)]^T$ is the predicted value of the state vector of the receiver at time k; $[\Delta\vec{u}(k|k), \Delta\vec{u}(k+1|k), \cdots, \Delta\vec{u}(k+N_u-1|k)]^T$ is the increment of the optimal control input of the receiver at moment k; N_p and N_u are respectively the lengths of the prediction and control time domains and $N_u \le N_p$; $Q = diag[q_1, q_2, \cdots, q_{12}]^T$, $R = diag[r_1, r_2, \cdots, r_6]^T$ and $S = diag[s_1, s_2, \cdots, s_{12}]^T$ are respectively the weight matrices of the corresponding states, control inputs and terminal states.

3.2 Constraint conditions

During the process of the receiver actively approaching the tanker, its movement speed, attitude and the control amount applied to it will all be subject to certain constraints and limitations. At the same time, considering that the two UAVs need to maintain a certain safety distance when approaching and the receiver is located directly behind and below the tanker, the specific constraint conditions are expressed as:

$$\vec{u}_{\min} \le \vec{u}(k+i-1|k) \le \vec{u}_{\max} \ (i = 1, 2, \cdots, N_u) \tag{30}$$

where the subscripts *min* and *max* are respectively represented as the upper and lower boundaries of the constraints.

$$\begin{cases} \vec{V}_{\min} \le \hat{\vec{V}}(k+i|k) \le \vec{V}_{\max} \\ \varphi_{\min} \le \hat{\varphi}(k+i|k) \le \varphi_{\max} \\ \theta_{\min} \le \hat{\theta}(k+i|k) \le \theta_{\max} \\ \psi_{\min} \le \hat{\psi}(k+i|k) \le \psi_{\max} \\ \vec{\omega}_{\min} \le \hat{\vec{\omega}}(k+i|k) \le \vec{\omega}_{\max} \end{cases} \qquad (i = 1, 2, \cdots, N_p) \tag{31}$$

$$\begin{cases} \sqrt{l_d^2 - (\Delta y)^2 - (\Delta z)^2} - \xi \le x_d(k+N_p|k) - \hat{x}(k+N_p|k) \le \sqrt{l_d^2 - (\Delta y)^2 - (\Delta z)^2} + \xi \\ \xi \le y_d(k+N_p|k) - \hat{y}(k+N_p|k) \le \xi \\ \sqrt{l_d^2 - (\Delta x)^2 - (\Delta y)^2} - \xi \le z_d(k+N_p|k) - \hat{z}(k+N_p|k) \le \sqrt{l_d^2 - (\Delta x)^2 - (\Delta y)^2} + \xi \\ \xi \le \vec{V}_d(k+N_p|k) - \hat{\vec{V}}(k+N_p|k) \le \xi \\ \xi \le \varphi_d(k+N_p|k) - \hat{\varphi}(k+N_p|k) \le \xi \\ \xi \le \theta_d(k+N_p|k) - \hat{\theta}(k+N_p|k) \le \xi \\ \xi \le \psi_d(k+N_p|k) - \hat{\psi}(k+N_p|k) \le \xi \end{cases} \tag{32}$$

where $\Delta x = x_d(k+N_p|k) - \hat{x}(k+N_p|k)$; $\Delta y = y_d(k+N_p|k) - \hat{y}(k+N_p|k)$; $\Delta z = z_d(k+N_p|k) - \hat{z}(k+N_p|k)$; l_d is the safe distance between the tanker and receiver; ξ is a minimum value greater than 0.

https://doi.org/10.1017/aer.2026.10233 Published online by Cambridge University Press

Given the initial state $\hat{\vec{X}}(0|0) = \vec{X}(0)$, combined with the dynamic model and constraint conditions, solving the optimal control variable $\vec{u}^*(t)$ so that the objective function J takes the minimum value.

3.3 Solution of the optimal control quantity

After establishing the prediction model for the motion control of the receiver, in order to obtain the optimal control quantity, the NMPC needs to solve a nonlinear optimisation problem shown in Equation (29) online in each control step. This paper will adopt the adaptive gradient descent method [5] to optimise the objective function online in order to obtain the optimal control quantity.

Let the state error $\vec{e}(k+i|k) = \vec{X}_d(k+i|k) - \hat{\vec{X}}(k+i|k)$, $(i = 1, 2, \cdots, N_p)$, and the objective function (29) can be rewritten as:

$$J = \sum_{i=1}^{N_p-1} \vec{e}^T(k+i|k) Q \vec{e}(k+i|k) + \sum_{i=0}^{N_u-1} (\Delta\vec{u})^T(k+i|k) R (\Delta\vec{u})(k+i|k) + \vec{e}^T(k+N_p|k) S \vec{e}(k+N_p|k) \tag{33}$$

Let $\vec{E}(k) = [\vec{e}(k+1|k), \vec{e}(k+2|k), \cdots, \vec{e}(k+N_p|k)]^T$ be the state error vector, $\Delta\vec{U}(k) = [\Delta\vec{u}(k|k), \Delta\vec{u}(k+1|k), \cdots, \Delta\vec{u}(k+N_u-1|k)]^T$ be the control input increment vector, $M = diag[Q_1, Q_2 \cdots, Q_{N_p-1}, S]^T$ is the state weight matrix, $H = diag[R_1, R_2 \cdots, R_{N_u}]^T$ be the control weight matrix, and then we have

$$J = \vec{E}^T(k) M \vec{E}(k) + (\Delta\vec{U})^T(k) H (\Delta\vec{U})(k) \tag{34}$$

The adaptive gradient descent method is adopted to optimise the objective function Equation (34), and the control increment vector $\Delta\vec{U}(k)$ can be obtained. The expression of gradient descent is:

$$\vec{U}(k+1) = \vec{U}(k) - \eta \frac{\partial J}{\partial \vec{U}(k)} = \vec{U}(k) + 2\eta \vec{P}^T(k) M \vec{E}(k) - 2\eta H (\Delta\vec{U})(k) \tag{35}$$

where η is the adaptive optimisation rate of the gradient descent method.

According to Equation (35), the control incremental vector $\Delta\vec{U}(k)$ can be obtained:

$$\Delta\vec{U}(k) = (1 + 2\eta H)^{-1} 2\eta \vec{P}^T(k) M \vec{E}(k) \tag{36}$$

where the expression of the matrix vector $\vec{P}(k)$ is

$$\vec{P}(k) = \begin{bmatrix} \frac{\partial \hat{\vec{X}}(k+1|k)}{\partial \vec{u}(k|k)} & 0 & \cdots & 0 \\ \frac{\partial \hat{\vec{X}}(k+2|k)}{\partial \vec{u}(k|k)} & \frac{\partial \hat{\vec{X}}(k+2|k)}{\partial \vec{u}(k+1|k)} & \cdots & 0 \\ \vdots & \vdots & \ddots & \vdots \\ \frac{\partial \hat{\vec{X}}(k+N_p|k)}{\partial \vec{u}(k|k)} & \frac{\partial \hat{\vec{X}}(k+N_p|k)}{\partial \vec{u}(k+1|k)} & \cdots & \frac{\partial \hat{\vec{X}}(k+N_p|k)}{\partial \vec{u}(k+N_u-1|k)} \end{bmatrix} \tag{37}$$

It can be deduced from the above that in the process of solving the control increment vector, the inversion and multiplication of matrices are involved, which increases the computational load and complexity of NMPC. Under normal circumstances, we choose the first control quantity $\vec{u}^*(k|k)$ in the control quantity $\vec{U}^*(k) = [\vec{u}^*(k|k), \vec{u}^*(k+1|k), \cdots, \vec{u}^*(k+N_u-1|k)]^T$ obtained through the optimisation solution as the control input quantity for the next optimisation solution [24]. Facts have proved that this choice can still enable NMPC to achieve satisfactory control effects [25]. Therefore, when the control time domain length N_u is set to 1, Equation (36) can be rewritten as:

$$\Delta\vec{u}(k|k) = (1 + 2\eta R_1)^{-1} 2\eta \vec{P}_1^T(k) Q_1 \vec{E}(k) \tag{38}$$

where $\vec{P}_1(k) = \left[\frac{\partial \hat{\vec{X}}(k+1|k)}{\partial \vec{u}(k|k)}, \frac{\partial \hat{\vec{X}}(k+2|k)}{\partial \vec{u}(k|k)}, \cdots, \frac{\partial \hat{\vec{X}}(k+N_p|k)}{\partial \vec{u}(k|k)} \right]^T$.

https://doi.org/10.1017/aer.2026.10233 Published online by Cambridge University Press

To accelerate the convergence speed of the gradient optimisation method, η can adaptively adjust in the real-time control process, namely [17]:

$$\eta_c = \frac{\kappa}{\lambda_{\max}\left(\vec{P}_1(k)\vec{P}_1^T(k)\right)} \tag{39}$$

where $0 < \kappa < 2$; $\lambda_{\max}$ is the maximum eigenvalue of $\vec{P}_1(k)\vec{P}_1^T(k)$.

Based on the above analysis, the optimal control increment $\Delta\vec{u}^*(k|k)$ can be expressed as:

$$\Delta\vec{u}^*(k|k) = \eta_c\vec{P}_1^T(k)\vec{E}(k) = \eta_c\sum\nolimits_{i=1}^{N_p}\left(\frac{\partial\hat{\vec{X}}(k+i|k)}{\partial\vec{u}(k|k)}\vec{e}(k+i|k)\right) \tag{40}$$

Substituting the optimal control increment $\Delta\vec{u}^*(k|k)$ into Equation (41), the optimal control quantity $\vec{u}^*(k)$ at time k can be obtained:

$$\vec{u}^*(k) = \vec{u}(k-1) + \Delta\vec{u}^*(k|k) \tag{41}$$

The optimal control quantity $\vec{u}^*(k)$ is input into the dynamic model of the receiver; the NMPC performs a new round of predictive control based on the motion state of the tanker/receiver at time $k+1$ until the control target requirements are met.

3.4 Stability analysis

Stability is a prerequisite for ensuring the normal operation of the control system. There are many methods for analysing the stability of control systems, such as Routhr's criterion, root locus method and Lyapunovr's theorem, etc. This paper will adopt the Lyapunov stability theorem to analyse the stability of the designed NMPC.

Selecting the Lyapunov quadratic positive definite function as shown in Equation (42):

$$\widehat{\vec{V}}(k) = \hat{\vec{E}}^T(k)\hat{\vec{E}}(k) \tag{42}$$

When the difference calculation is performed on Equation (42), there is

$$\begin{aligned}\Delta\widehat{\vec{V}}(k) &= \widehat{\vec{V}}(k+1) - \widehat{\vec{V}}(k)\\ &= \hat{\vec{E}}^T(k+1)\hat{\vec{E}}(k+1) - \hat{\vec{E}}^T(k)\hat{\vec{E}}(k)\\ &= \left[\hat{\vec{E}}^T(k) + \Delta\hat{\vec{E}}^T(k)\right]\left[\hat{\vec{E}}(k) + \Delta\hat{\vec{E}}(k)\right] - \hat{\vec{E}}^T(k)\hat{\vec{E}}(k)\\ &= \Delta\hat{\vec{E}}^T(k)\left[2\hat{\vec{E}}(k) + \Delta\hat{\vec{E}}(k)\right]\end{aligned} \tag{43}$$

Since $\vec{E}(k) = [\vec{e}(k+1|k), \vec{e}(k+2|k), \cdots, \vec{e}(k+N_p|k)]^T$, then there is

$$\frac{\partial\hat{\vec{E}}(k)}{\partial\vec{u}(k|k)} = -\left[\frac{\partial\hat{\vec{X}}(k+1|k)}{\partial\vec{u}(k|k)}, \frac{\partial\hat{\vec{X}}(k+2|k)}{\partial\vec{u}(k|k)}, \cdots, \frac{\partial\hat{\vec{X}}(k+N_p|k)}{\partial\vec{u}(k|k)}\right]^T = -\vec{P}_1(k) \tag{44}$$

Therefore, $\Delta\hat{\vec{E}}(k)$ can be expressed as:

$$\Delta\hat{\vec{E}}(k) = \frac{\partial\hat{\vec{E}}(k)}{\partial\vec{u}(k|k)}\Delta\vec{u}(k|k) = -\eta_c\vec{P}_1(k)\vec{P}_1^T(k)\hat{\vec{E}}(k) \tag{45}$$

Substituting Equation (45) into Equation (43) and rearranging, we can obtain:

$$\begin{aligned}\Delta\widehat{\vec{V}}(k) &= -\eta_c\left[\vec{P}_1(k)\vec{P}_1^T(k)\hat{\vec{E}}(k)\right]^T\left[2\hat{\vec{E}}(k) - \eta_c\vec{P}_1(k)\vec{P}_1^T(k)\hat{\vec{E}}(k)\right]\\ &= -\eta_c\hat{\vec{E}}^T(k)\vec{P}_1^T(k)\vec{P}_1(k)\left[2\vec{I} - \eta_c\vec{P}_1(k)\vec{P}_1^T(k)\right]\hat{\vec{E}}(k)\end{aligned} \tag{46}$$

From Equation (44), it can be known that $0 < \eta_c\lambda_{\max}(\vec{P}_1(k)\vec{P}_1^T(k)) = \kappa < 2$, then $\Delta\widehat{\vec{V}}(k) < 0$, which can prove that the designed NMPC method is theoretically stable and convergent.

https://doi.org/10.1017/aer.2026.10233 Published online by Cambridge University Press

Table 1. *Configuration of high-performance computers*

Name	Specification model	Name	Specification model
Processor	Intel i7-13700KF	Main frequency	2.7 GHz
Motherboard	Asus ROG Z790-A	Graphics card	Raptor ROG-STRIX-RTX 4084-O16G-W
Memory	G.skill (16G*4) DDR5 7200	Hard disk	2T*2 PCIE solid-state Samsung 990Pro
Power supply	ROG STRIX Blowing Snow 1000W	Heat dissipation	ROG Rozen III 360ARGB white water cooler

Table 2. *Physical parameters of the dynamic model [26, 27]*

Variable	Value	Variable	Value
Quality m	2400 kg	Wing area S	8 m^2
Wing span b	12 m	Average aerodynamic chord length of the wing c	6 m
Moment of inertia J_x	5.0×10^{-3} kg × m^2	Moment of inertia J_y	5.0×10^{-3} kg × m^2
Moment of inertia J_z	8.9×10^{-3} kg × m^2	Moment of inertia J_{xz}	0.006×10^{-3} kg × m^2

Table 3. *Aerodynamic coefficient of the dynamic model [28]*

Variable	Value	Variable	Value	Variable	Value	Variable	Value	Variable	Value
C_{L_0}	0.400	C_{L_α}	2.000	$C_{L_{\omega_y}}$	−0.100	$C_{L_{\delta_e}}$	0.002	$C_{D_{\omega_x}}$	−0.100
$C_{D_{\omega_y}}$	−0.100	$C_{D_{\delta_e}}$	0.001	C_{Y_0}	0.150	C_{Y_β}	1.000	$C_{Y_{\omega_x}}$	−0.100
$C_{Y_{\omega_z}}$	−0.100	$C_{Y_{\delta_a}}$	0.004	$C_{Y_{\delta_r}}$	0.003	C_{x_0}	0.150	C_{x_β}	1.500
$C_{x_{\omega_x}}$	−0.050	$C_{x_{\omega_z}}$	−0.050	$C_{x_{\delta_a}}$	0.001	$C_{x_{\delta_r}}$	0.002	C_{y_0}	0.200
C_{y_α}	1.500	$C_{y_{\omega_y}}$	−0.070	$C_{y_{\delta_e}}$	0.001	C_{z_0}	0.250	C_{z_β}	2.000
$C_{z_{\omega_x}}$	−0.070	$C_{z_{\omega_z}}$	−0.070	$C_{z_{\delta_a}}$	0.002	$C_{z_{\delta_r}}$	0.003	ρ	1.293 kg/m^3

4.0 Numerical simulation and result analysis

To verify the control performance of the NMPC method established in this paper during the active approach of the receiver to the tanker, a certain type of UAV was taken as the controlled object, and numerical simulation and result analysis were carried out in the Matlab/Simulink environment on a high-performance desktop computer. The configuration of the high-performance desktop computer is shown in Table 1 as follows.

4.1 Parameter initialization

The tanker is assumed to maintain straight and level flight at a constant speed. In the geocentric coordinate system, the initial positions of the tanker are (4.25, 12, 6.58) km, the flight speed is 25 m/s, and the attitude angles (φ, θ, ψ) are (0, 0, 0) degrees, respectively. In order to verify the effectiveness of the proposed method, the three initial positions of the receiver are be given as (0, 0, 5) km (condition 1), (1, 2, 3) km (condition 2) and (2, 2.5, 5) km (condition 3), the initial speed is 30 m/s, and the initial attitude angles $(\varphi_0, \theta_0, \psi_0)$ are (0, 0, 66) degrees, respectively. The physical parameters and aerodynamic coefficient initialisations of the dynamic model of the receiver are shown in Tables 2 and 3, respectively.

The conditions that the receiver is subject to during its flight are shown in Table 4 as follows.

https://doi.org/10.1017/aer.2026.10233 Published online by Cambridge University Press

Table 4. *Variable constraints [29, 30]*

Variable	Minimum value	Maximum value	Variable	Minimum value	Maximum value
Speed V	0	120m/s	Rolling angle φ	$-180°$	$180°$
Pitch angle θ	$-180°$	$180°$	Yaw angle ψ	$-180°$	$180°$
Engine thrust f	0	124.50kN	Aileron rudder deflection angle δ_a	$-35°$	$35°$
Elevator deflection angle δ_e	$-35°$	$35°$	Rudder deflection angle δ_r	$-35°$	$35°$

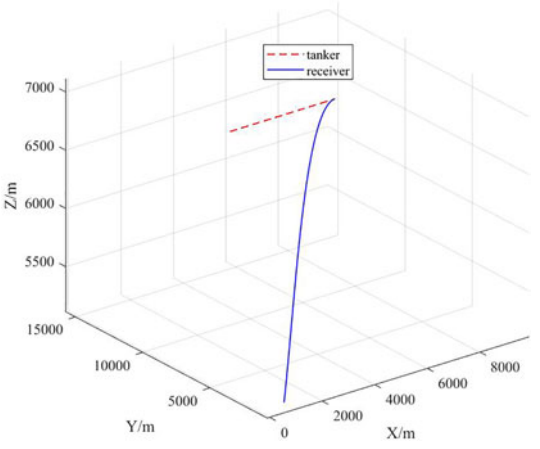


Figure 1. *Rendezvous trajectory in condition 1.*

Our goal is that, based on the above parameters and constraints, the receiver will eventually fly at the same speed and in the same direction as the tanker and be located directly below and behind the tanker.

4.2 Simulation result analysis

Suppose the length of the prediction domain $N_p = 20$ and the length of the control domain $N_u = 1$, the receiver eventually flies forward parallel to the ground horizontal line at a constant speed of 25 m/s, and the deviation between the flight position and the position of the tanker is $\Delta = (-0.05, 0.0, -0.08)$ km. According to the settings of the parameters in section 4.1, the numerical simulation results are as follows.

Figures 1–6 present the motion trajectory and the three-axis position errors of the tanker/receiver during autonomous approach and rendezvous with three different conditions, respectively. It can be seen from that although the initial positions of the receiver is different, the receiver can quickly achieve autonomous approach and rendezvous with the tanker, and the three-axis errors between the receiver and the tanker are eventually stabilized at -50 m, 0 m and -80 m, respectively, indicating that the receiver is directly below and behind the tanker, meeting the flight position requirements set by the numerical simulation.

Figures 7–10 present the change curves of flight speed, roll angle, pitch angle and yaw angle during the autonomous approach of the receiver to the tanker in condition 1, respectively. It can be seen that the receiver flies at an initial speed of 30 m/s, after approximately 30 s, it begins to reach the maximum speed of 115 m/s, and then flies towards the tanker at the maximum speed independently. After approximately 100 s, the receiver begins to decelerate and fly towards the tanker. Finally, after around 150 s, it decelerates to 25 m/s and maintains the same flight speed as the tanker. After a period of change, the

https://doi.org/10.1017/aer.2026.10233 Published online by Cambridge University Press

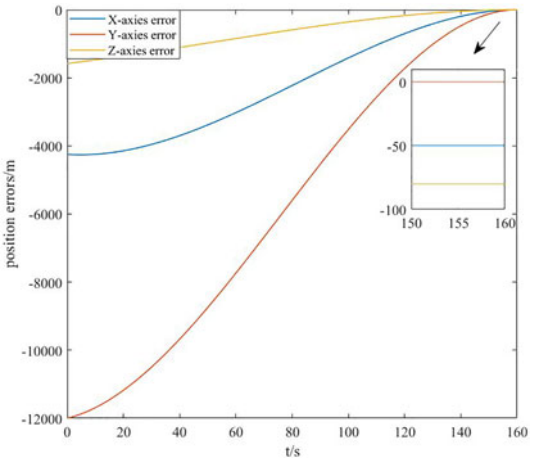


Figure 2. *The position errors of the three axes of the tanker/receiver.*

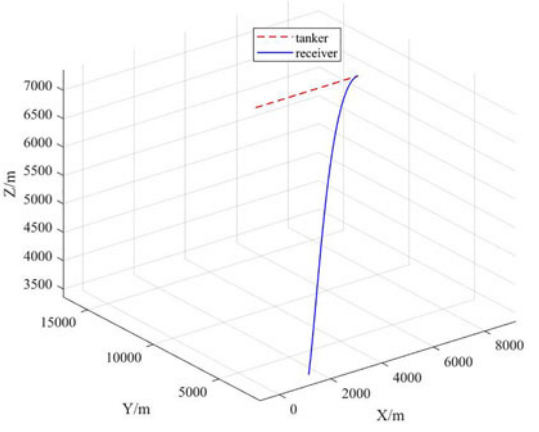


Figure 3. *Rendezvous trajectory in condition 2.*

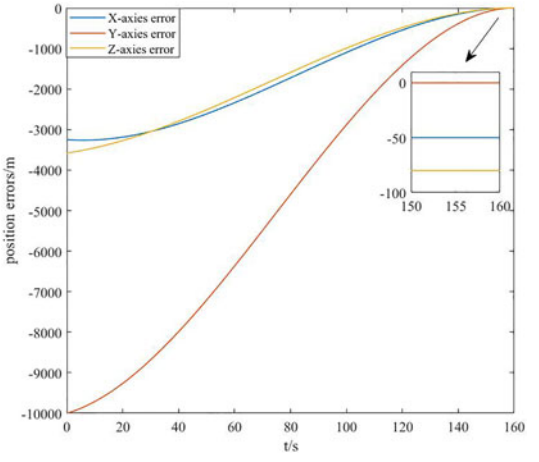


Figure 4. *The position errors of the three axes of the tanker/receiver.*

https://doi.org/10.1017/aer.2026.10233 Published online by Cambridge University Press

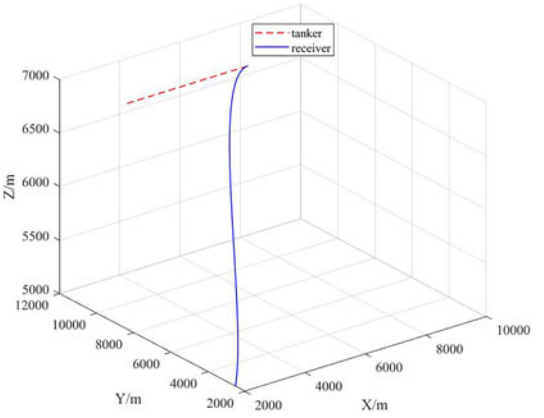


Figure 5. *Rendezvous trajectory in condition 3.*

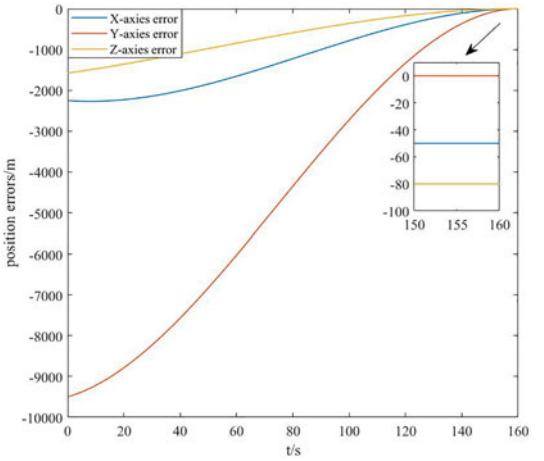


Figure 6. *The position errors of the three axes of the tanker/receiver.*

flight attitude angle of the receiver remains consistent with that of the tanker at about 150 s. That is, the receiver eventually maintains the same flight direction as the tanker, meeting the requirements of the flight speed and direction of the tanker/receiver.

Taking into account the impact of atmospheric turbulence on the tanker and receiver, a simulation is conducted to verify the control performance of the proposed method under turbulence effects. The simulation results are presented in Figures 11 and 12. It can be seen that although atmospheric turbulence can have a certain impact, the receiver is directly below and behind the tanker, meeting the flight position requirements set by the numerical simulation, indicating the control stability of the proposed method.

To further verify the control performance of the proposed method, the relative distance between the tanker and the receiver is taken as the performance indicator. The simulation comparison results between the proposed method, LQR and MPC are shown in Figure 13. As seen in the figure, the NMPC-based control performance is the best.

The simulation results show that the proposed method can meet the requirements for autonomous approach and rendezvous between the receiver and the tanker. The receiver can maintain a position directly behind and below the tanker while flying at the same speed as the tanker. The established method has good control performance, verifying its effectiveness.

https://doi.org/10.1017/aer.2026.10233 Published online by Cambridge University Press

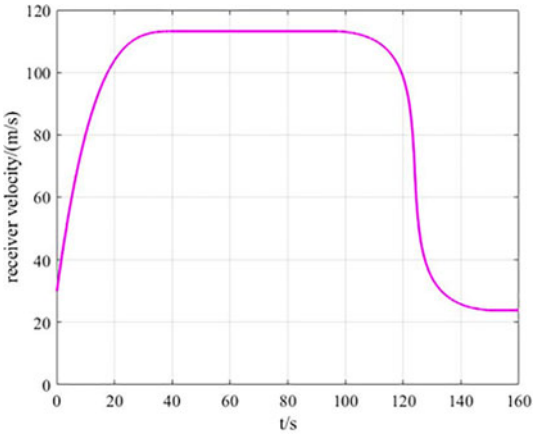


Figure 7. *The flight speed of the receiver.*

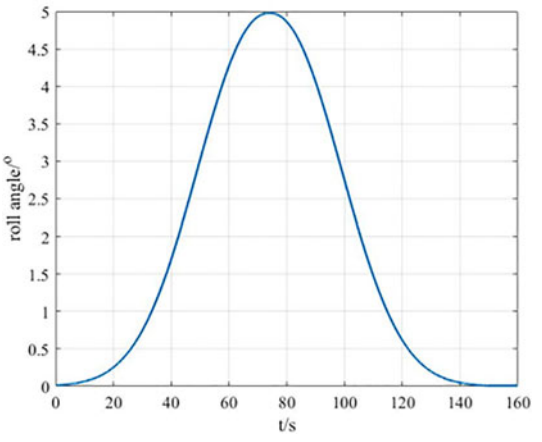


Figure 8. *The rolling angle of the receiver.*

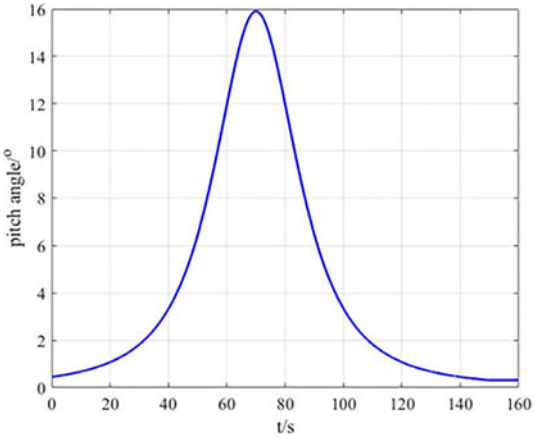


Figure 9. *The pitch angle of the receiver.*

https://doi.org/10.1017/aer.2026.10233 Published online by Cambridge University Press

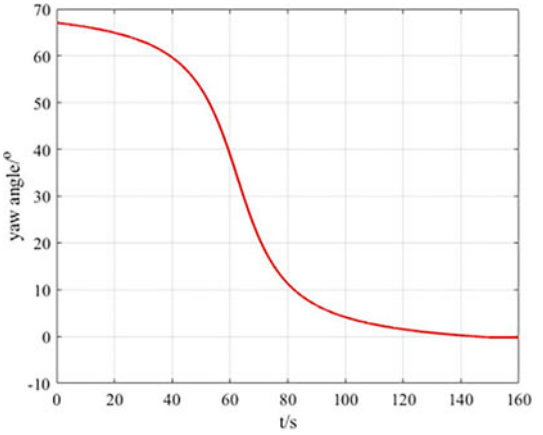


Figure 10. *The yaw angle of the receiver.*

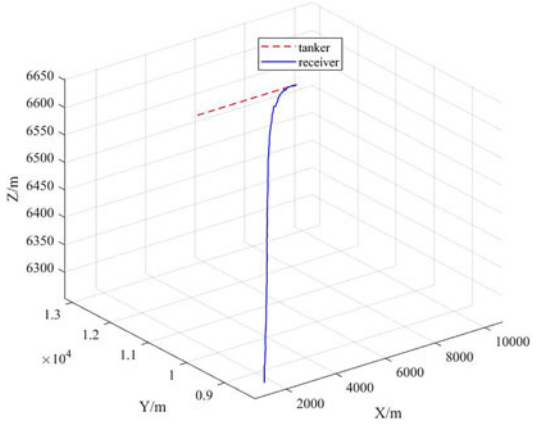


Figure 11. *Rendezvous trajectory under turbulence.*

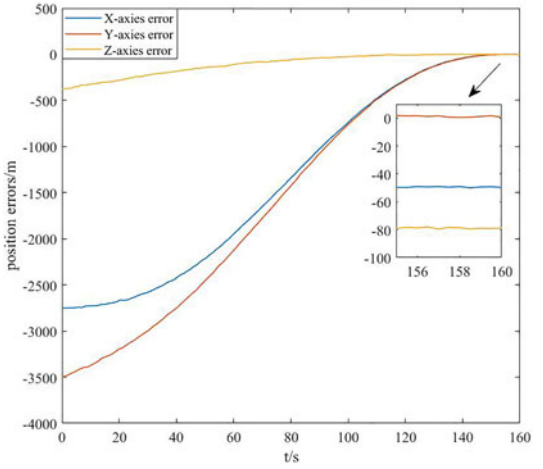


Figure 12. *The position errors of the three axes of the tanker/receiver.*

https://doi.org/10.1017/aer.2026.10233 Published online by Cambridge University Press

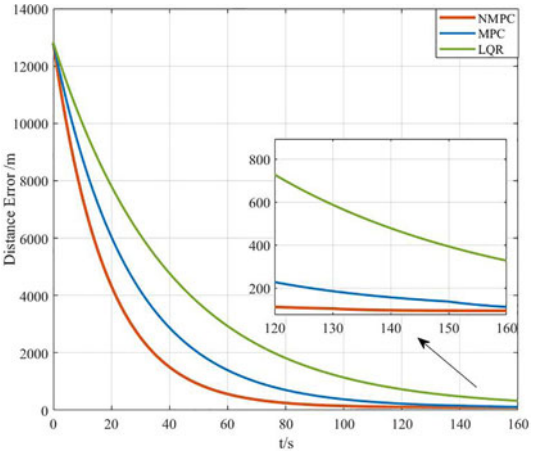


Figure 13. *The comparison results with different methods.*

5.0 Conclusion

In this paper, an autonomous approach and rendezvous method for unmanned tanker/receiver based on NMPC is established. Through the analysis and modelling of the resultant external force and torque acting on the receiver during its motion process, appropriate state variables and control variables are selected to establish a nonlinear dynamic model of the entire state of the receiver. The objective function with state terminals is designed by applying the NMPC theory. Combined with the constraint conditions, the adaptive gradient descent method is adopted to solve the optimal control quantity online, and the stability analysis is carried out. Numerical simulation verifies the control performance of the established method.

The simulation results show that the established method can quickly achieve the autonomous approach and rendezvous of the tanker and receiver in the air, ensuring that the receiver maintains the same speed and direction as the tanker directly behind and below it. The established method features high control accuracy, stable control process and excellent control performance.

Data and materials availability. The authors confirm that the data supporting the findings of this study are available within the article.

Acknowledgements. This work is supported by the Natural Science Basic Research Program-General Projects-Youth Projects of Shaanxi Provincial Department of Science and Technology under Grant No. 2025JC-YBQN-944, the Natural Science Basic Research Program-General Projects-Surface Projects of Shaanxi Provincial Department of Science and Technology under Grant No. 2025JC-YBMS-746, the Scientific Research Plan Project of the Education Department of Shaanxi Province-Youth Innovation Team Project under Grant No. 23JP071 and the Doctoral Research Foundation of Xihang University under Grant No. 2024KY0210. The authors would like to thank all editors and anonymous reviewers for improving this article.

Author contribution. H.S. was responsible for experimental conceptualisation and design, and was the main contributor to writing the manuscript; H.F., S.S.S. and X.Y.W. reviewed and revised the manuscript, and verified the experimental design; R.H.D. analysed and explained the experimental data. All authors have reviewed the manuscript.

Competing interests. The authors declare no competing interests.

References

[1] Rasol, J., Yuelei, X.U., Qing, Z., et al. N-fold bernoulli probability based adaptive fast-tracking algorithm and its application to autonomous aerial refueling, *Chin. J. Aeronaut.*, 2023, **36**, pp 356–368.

[2] Lee, S. and Kim, M. Analysis of rendezvous guidance laws for autonomous aerial refueling for non-maneuvering and identical speed targets, *Aerosp. Sci. Technol.*, 2022, **121**, p 107359.

https://doi.org/10.1017/aer.2026.10233 Published online by Cambridge University Press

[3] Weijia, X. *Research on UAV Aerial Refueling Rendezvous Route Based on Nonlinear Guidance Law*, University of Electronic Science and Technology of China, 2020 (in Chinese).
[4] Burns, B., Blue, P. and Zollars, M. *Autonomous Control for Automated Aerial Refueling with Minimum-time Rendezvous*, AIAA Guidance, Navigation and Control Conference and Exhibit, 2007, p 6739.
[5] Lugo-Cárdenas, I., Flores, G., Salazar, S., et al. Dubins path generation for a fixed-wing UAV, *2014 International Conference on Unmanned Aircraft Systems (ICUAS). IEEE*, 2014, pp 339–346.
[6] Owen, M., Nichols, J. and Colton, M. *Cooperative Aerial Tracking and Rendezvous along Time-optimal 3-Dimensional Curves*, AIAA Guidance, Navigation, and Control Conference, 2011, p 6546.
[7] Ochi, Y. and Kominami, T. *Flight Control for Automatic Aerial Refueling via PNG and LOS Angle Control*, AIAA Guidance, Navigation, and Control Conference and Exhibit, 2005, p 6268.
[8] Smith, A.L. Proportional navigation with adaptive terminal guidance for aircraft rendezvous, *J. Guid. Control Dyn.*, 2008, **31**, pp 1832–1836.
[9] Yoon, Y., Kim, M. and Kim, Y. Three-dimensional path planning for aerial refueling between one tanker and multiple UAVs, *Int. J. Aeronaut. Space Sci.*, 2018, **19**, pp 1027–1040.
[10] Kung, C.C., Chiang, F.L. and Chen, K.Y. Design a three-dimensional pursuit guidance law with feedback linearization method, *Int. J. Aerosp. Mech. Eng.*, 2011, **5**, pp 1210–1215.
[11] Jun, G. and Xinming, D. Design of UAV autonomous controller for rendezvous in aerial refueling, *Control Decis.*, 2010, **25**, pp 567–571 (in Chinese).
[12] Dogan, A. and Venkataramanan, S. Nonlinear control for reconfiguration of unmanned-aerial-vehicle formation [J], *J. Guid. Control Dyn.*, 2005, **28**, pp 667–678.
[13] Schumacher, C.J. and Kumar, R. Adaptive control of UAVs in close-coupled formation flight, *Proceedings of the 2000 American Control Conference. ACC (IEEE Cat. No. 00CH36334).* IEEE, 2000, **2**, pp 849–853.
[14] Quanquan, G., Suozhong, Y. and Jin, Z. Guidance and control of autonomous aerial refueling rendezvous trajectory chasing based on sliding mode method, *J. Appl. Sci.-Electron. Inform. Eng.*, 2016, **34**, pp 215–226 (in Chinese).
[15] Suozhong, Y., Xinhua, W. and Fengying, Z. Guidance and control of autonomous aerial refueling rendezvous, *Flight Dyn.*, 2014, **32**, pp 20–24 (in Chinese).
[16] Xiaoqi, Q. *Research On Robust Disturbance Rejection Control Of Moving Mass Fixed-Wing Unmanned Aerial Vehicle*, Harbin Institute of Technology, 2020 (in Chinese).
[17] Hongbiao, Z., Yu, Z., Xiaoying, B., et al. Model predictive control of nonlinear system based on adaptive fuzzy neural network, *CIESC J.*, 2020, **71**, pp 3201–3212 (in Chinese).
[18] Sixu, L., Biao, X., Manjiang, H., et al. A dynamic model predictive control approach for multipoint preview path tracking of articulated vehicles, *Autom. Eng.*, 2021, **43**, pp 1187–1194 (in Chinese).
[19] Hongwei, W., Chenyu, L., Lei, L., et al. Research on trajectory tracking control of unmanned vehicle based on efficient NMPC algorithm, *Autom. Eng.*, 2022, **44**, pp 1494–1502+1618 (in Chinese).
[20] Chen, L., Liu, M., Shi, Y., et al. Adaptive fault estimation for unmanned surface vessels with a neural network observer approach, *IEEE Trans. Circ. Syst. I: Regular Pap.*, 2020, **68**, pp 416–425.
[21] Bolian, Z. *Docking Control Method for Autonomous Aerial Refueling for Unmanned Aerial Vehicles*, Harbin Institute of Technology, 2018 (in Chinese).
[22] Xiaoqi, Q., Changsheng, G. and Wuxing, J. Dynamic analysis and disturbance rejection control of mass-actuated fixed-wing UAV, *J. Beijing Univ. Aeronaut. Astronaut.*, 2022, **48**, pp 430–437 (in Chinese).
[23] Chen, C. and Tan, J. Path following for UAV using nonlinear model predictive control, *J. Phys.: Conf. Series*, 2023, **2530**, p 012021.
[24] Sun, N., Zhang, W. and Yang, J. Integrated path tracking controller of underground articulated vehicle based on nonlinear model predictive control, *Appl. Sci.*, 2023, **13**, p 5340.
[25] Lu, C. Wavelet fuzzy neural networks for identification and predictive control of dynamic systems, *IEEE Trans. Ind. Electron.*, 2011, **58**, pp 3046–3058.
[26] Slegers, N., Kyle, J. and Costello, M. Nonlinear model predictive control technique for unmanned air vehicles, *J. Guid. Control Dyn.*, 2006, **29**, pp 1179–1188.
[27] Xu, Q., Wang, Z. and Li, Y. Fuzzy adaptive nonlinear information fusion model predictive attitude control of unmanned rotorcrafts [J], *Aerosp. Sci. Technol.*, 2020, **98**, p 105686.
[28] Ostowari, C. and Naik, D. Post-stall wind tunnel data for NACA 44XX series airfoil sections, *Texas A and M Univ., College Station (USA). Dept. of Aerospace Engineering*, 1985.
[29] Reinhardt, D. and Johansen, T.A. Control of fixed-wing uav attitude and speed based on embedded nonlinear model predictive control, *IFAC-PapersOnLine*, 2021, **54**, pp 91–98.
[30] Mathisen, S., Gryte, K., Gros, S., et al. Precision deep-stall landing of fixed-wing UAVs using nonlinear model predictive control, *J. Intell. Robot. Syst.*, 2021, **101**, pp 1–15.

Cite this article: Song H., Fan H., Di R., Wang X. and Shi S. Nonlinear model predictive control method for autonomous approach of tanker/receiver. *The Aeronautical Journal*, https://doi.org/10.1017/aer.2026.10233

https://doi.org/10.1017/aer.2026.10233 Published online by Cambridge University Press